Advantages of Square-Root Extended Kalman Filter for Sensorless Control of AC Drives

Václav Šmídl, *Member, IEEE*, and Zdeněk Peroutka, *Member, IEEE*

***Abstract*—This paper is concerned with a fixed-point implementation of the extended Kalman filter (EKF) for applications in sensorless control of ac motor drives. The sensitivity of the EKF to round-off errors is well known, and numerically advantageous implementations based on the square-root decomposition of covariance matrices have been developed to address this issue. However, these techniques have not been applied in the EKF-based sensorless control of ac drives yet. Specific properties of the fixed-point implementation of the EKF for a permanent-magnet synchronous motor (PMSM) drive are presented in this paper, and suitability of various square-root algorithms for this case is discussed. Three square-root algorithms—Bierman–Thorton, Carlson–Schmidt–Givens, and Carlson–Schmidt–Householder—were implemented, and their performances are compared to that of the standard implementation based on full covariance matrices. Results of both simulation studies and experimental tests performed on a developed sensorless PMSM drive prototype of rated power of 10.7 kW are presented. It was confirmed that the square-root algorithms improve the behavior of the sensorless control in critical operating conditions such as low speeds and speed reversal. In particular, the Carlson–Schmidt–Givens algorithm was found to be well suited for the considered drive.**

***Index Terms*—AC motors, Kalman filter, parameter estimation, sensorless control, variable-speed drives.**

I. Introduction

OPERATION of an ac drive without either rotor position or speed sensor—the so-called sensorless control—is a very popular topic in the literature. Many techniques allowing sensorless estimation of the rotor speed and its position using anisotropy-based [1]–[8] or model-based methods [9]–[16] have been published. However, robust sensorless control of the drive under critical operating conditions such as standstill, low speeds, and failure states is still a challenge. The most popular model-based estimator allowing sensorless drive control in a wide speed range (including very low speeds) is the extended Kalman filter (EKF) [17]–[25]. The EKF is widely understood to be an algorithm requiring high computational performance of a digital signal processor (DSP) and complicated tuning [26]. Powerful floating-point DSPs or field-programmable gate arrays are used in most of the applications of EKF; this is a well-documented "conventional task" [24], [27], [28]. Implementation of the EKF in a fixed-point DSP with limited computational performance—which is, at present, used in ac electric drives from simple consumer electronics up to either traction or generally high-power drives—is much more demanding. The fixed-point arithmetic implies limited dynamic range and scales and, therefore, reduced calculation accuracy. A specific issue of the EKF is overflowing of covariance matrices and the necessity of their saturations. Reduced accuracy of the fixed-point implementation severely affects the performance of the EKF under critical operating conditions. Therefore, we seek an implementation of the EKF offering higher numerical precision without an excessive computational cost.

Calculation of the EKF equations with covariance matrices in full representation is the most common and widely disseminated approach [18], [29]. This approach is known to potentially suffer from numerical instability due to round-off errors. Better numerical stability can be achieved when the covariance matrices are represented in their square-root decompositions [30]. The two popular choices of the square-root form are the Cholesky decomposition and the UD decomposition. Several variants of algorithms evaluating the Kalman filter equations using these decompositions are available in the literature (see [30] for survey and [31] for the latest development). Each variant has advantages and drawbacks that make each of them suitable for different kinds of models and computational platforms. The purpose of this paper is to investigate the suitability of the square-root algorithms for ac motor drives and 16-/32-b fixed-point microcontrollers. The square-root EKF has been implemented for sensorless drive control only in floating-point arithmetic [22]. No publication on the fixed-point square-root EKF sensorless drive control is known to us.

The presented square-root EKF is generally suitable for all kinds of ac motor drives, such as permanent-magnet synchronous motor (PMSM) or induction motor drive. Properties of the investigated fixed-point square-root EKF and its application benefits will be studied on a drive with surface-mounted PMSM in this paper. Selection of the PMSM drive has been motivated by our recent research of a new generation of trams with gearless wheel drive with PMSMs [32]. The drive diagnostic

Manuscript received December 30, 2010; revised May 11, 2011 and July 18, 2011; accepted December 1, 2011. Date of publication December 16, 2011; date of current version June 19, 2012. This work was supported in part by the European Regional Development Fund and Ministry of Education, Youth and Sports of the Czech Republic under Project CZ.1.05/2.1.00/03.0094: Regional Innovation Centre for Electrical Engineering and in part by the Czech Science Foundation under Project P102/11/0437.

V. Šmídl is with the Regional Innovation Centre for Electrical Engineering, University of West Bohemia, 30614 Plzeň, Czech Republic, and also with the Institute of Information Theory and Automation, The Academy of Sciences of the Czech Republic, 18208 Prague, Czech Republic (e-mail: vsmidl@rice.zcu.cz).

Z. Peroutka is with the Regional Innovation Centre for Electrical Engineering, University of West Bohemia, 30614 Plzeň, Czech Republic (e-mail: peroutka@ieee.org).

Color versions of one or more of the figures in this paper are available online at http://ieeexplore.ieee.org.

Digital Object Identifier 10.1109/TIE.2011.2180273

requires the estimation of the rotor position without either rotor position or speed sensor in a very wide speed range. The EKF was selected for this task.

This paper is organized as follows. The classical EKF algorithm for the PMSM drive and its square-root variants are introduced in Section II. Details of fixed-point implementation of all considered algorithms are discussed in Section III. The presented algorithms are compared in simulations and experiments on a sensorless PMSM drive of rated power of 10.7 kW in Section IV.

II. EKF Design for Investigated PMSM Drive

A. Mathematical Model of PMSM

A commonly used model of a PMSM is the stationary reference frame model discretized using the first-order Euler formula for a time step Δt

$$\begin{aligned} i_{s\alpha,t+1} &= \left(1 - \frac{R_s}{L_s}\Delta t\right) i_{s\alpha,t} + \frac{\Psi_{\mathrm{pm}}}{L_s}\Delta t \omega_{me,t} \sin \vartheta_{e,t} \\ &\quad + u_{s\alpha,t}\frac{\Delta t}{L_s}, \\ i_{s\beta,t+1} &= \left(1 - \frac{R_s}{L_s}\Delta t\right) i_{s\beta,t} - \frac{\Psi_{\mathrm{pm}}}{L_s}\Delta t \omega_{me,t} \cos \vartheta_{e,t} \\ &\quad + u_{s\beta,t}\frac{\Delta t}{L_s}, \\ \omega_{me,t+1} &= \omega_{me,t}, \\ \vartheta_{e,t+1} &= \vartheta_{e,t} + \omega_{me,t}\Delta t. \end{aligned} \tag{1}$$

Here, $i_{s\alpha}$, $i_{s\beta}$, $u_{s\alpha}$, and $u_{s\beta}$ represent the components of the stator current and voltage vector in the stationary reference frame, respectively, ω_{me} is the electrical rotor speed, and ϑ_e is the electrical rotor position. R_s and L_s are the stator resistance and inductance, respectively, Ψ_{pm} is the flux linkage excited by permanent magnets on the rotor, and Δt is the sampling period. The third equation of (1) is simplified; we assume that the speed change within one sampling period is negligible.

The equations in (1) represent the nonlinear state-space model of PMSM with state vector $x_t = [i_{s\alpha,t}, i_{s\beta,t}, \omega_{me,t}, \vartheta_{e,t}]$. The equations are subject to errors which may be caused by inaccurate linearization, uncertainties in parameters (e.g., due to temperature changes and saturation), unobserved physical effects (such as the unknown load, dead-time effects, and nonlinear voltage drops on power electronics devices), and others [33]. For consistency with the EKF assumptions, all of these errors are assumed to influence the state equations as an additive noise with Gaussian distribution. Generally, it is assumed that the noise between the state variables is uncorrelated and its variance is constant $Q = \mathrm{diag}(q_i, q_i, q_\omega, q_\vartheta)$.

The variance of the observation error, $R = [r_i,\ r_i]$, can be derived from the properties of the data acquisition system [33].

B. Background of Extended Kalman Filtering

The EKF is a stochastic filter that recursively computes the expected value of the state variable $\hat{x}_t$ and its associated covariance matrix P_t. Recursive computation of these quantities is often split into two steps.

1) **Prediction**: Compute the time evolution of the estimates from time t to $t+1$, $\hat{x}_{t+1}^{\mathrm{pred}} = g(\hat{x}_t)$, where $g()$ is given in (1), and the covariance matrix of the predictions is

$$S_{t+1} = A_t P_t A_t^{\mathrm{T}} + Q_t \tag{2}$$

$$A_t = \frac{\partial x_{t+1}(x_t)}{\partial x_t}. \tag{3}$$

2) **Correction**: Compute the prediction of the observations $\hat{y}_t = [\hat{i}_{s\alpha,t}, \hat{i}_{s\beta,t}]$, and adjust the estimates of the state and its variance

$$P_t = (I - K_t C_t) S_{t+1} \tag{4}$$

$$K_t = S_{t+1} C_t \left(C_t S_{t+1} C_t^{\mathrm{T}} + R\right)^{-1} \tag{5}$$

$$\begin{aligned} \hat{x}_{t+1} &=, \hat{x}_{t+1}^{\mathrm{pred}} + K_t(y_t - \hat{y}_t), \\ C &= \frac{\partial y_t}{\partial x_t}. \end{aligned} \tag{6}$$

For model (1), the matrix of derivatives A_t (3) is

$$A = \begin{bmatrix} a & & b\sin\vartheta_{e,t} & c\cos\vartheta_{e,t} \\ & a & -b\cos\vartheta_{e,t} & c\sin\vartheta_{e,t} \\ & & 1 & \\ & & \Delta t & 1 \end{bmatrix}$$

where $a = (1 - (R_s/L_s)\Delta t)$, $b = (\Psi_{\mathrm{pm}}/L_s)\Delta t$, and $c = (\Psi_{\mathrm{pm}}/L_s)\Delta t\omega_{me,t}$. The matrix C is

$$C = \begin{bmatrix} 1 & 0 & 0 & 0 \\ 0 & 1 & 0 & 0 \end{bmatrix}.$$

C. Square-Root Kalman Filtering

The original filtering equations (2)–(6) are typically unsuitable for numerical implementations due to propagation of round-off errors. Alternative forms of (2)–(6) have been studied for numerical stability, and extensive knowledge in this field has been accumulated (see, e.g., [30] for detailed background).

The key property that needs to be maintained is the symmetry and positive definiteness of covariance matrices P_t and S_t at all time steps. This requirement is hard to achieve when the matrix is stored as a 4×4 array of numbers. More efficient representation of the covariance matrices is based on the Cholesky decomposition or the modified Cholesky decomposition. For example, the Cholesky decomposition of the covariance matrix of estimates P_t is

$$P_t = G_t G_t^{\mathrm{T}} \tag{7}$$

where G_t is a lower triangular matrix. The modified Cholesky decomposition (also known as the UD decomposition) is

$$P_t = U_t D_t U_t^{\mathrm{T}} \tag{8}$$

where U_t is the unit upper triangular (its diagonal is formed by a unit vector) and D is diagonal. Decompositions (7) and (8) represent two basic choices in matrix representation. For each of these choices, all covariance matrices (i.e., Q, R, and S) are represented in the same form, and (2)–(4) are rederived in this parametrization. Many variants of these square-root algorithms are known; however, we will consider only the following three of them.

1) Bierman–Thorton method based on representing the covariance matrices in UD form (8) and evaluation of (2) using the modified Gramm-Schmidt orthogonalization method. The method first computes matrix $A_t U_t$ which is passed to the Thorton algorithm evaluating (2) and then to the Bierman algorithm evaluating (4).
2) Carlson–Schmidt–Givens algorithm representing the covariance matrices in the Cholesky decomposition (7) and evaluating (2) using Givens rotations. The method first computes matrix $A_t G_t^{\mathrm{T}}$, which is transformed into the Cholesky decomposition of S_t (2). The result is updated by the Carlson algorithm.
3) Carlson–Schmidt–Householder algorithm is computed in the same way as the previous one with the exception of computation of S_t via (2), which is computed using Householder reflections.

In general, it is not possible to decide which algorithm will work best for a given system. In this paper, we implement all of them and compare them empirically.

III. Fixed-Point Implementation

Floating-point implementations of all three considered square-root algorithms are available in [30] and accompanied with evaluation of their computational complexity. Fixed-point implementations of these algorithms were reported to be advantageous in other domains, e.g., [34]. We present a detailed analysis of their application to the ac motor drive (in our case, PMSM) model and outline its specific features that were taken into account.

A. Transformation to Scaled Variables

The challenge for any fixed-point implementation is to find bounds on all involved quantities. It is easy for the state variables which have physical meaning and known physical bounds. For example, the current $i_{s\alpha}$ is bounded by $\langle -i_{s,\max}, i_{s,\max}\rangle$ and can be represented by

$$\bar{i}_{s\alpha} = \frac{i_{s\alpha}}{i_{s,\max}} \in \langle -1, 1\rangle \tag{9}$$

that can be trivially represented in any chosen precision. Analogically, the state variables x_t can be normalized to $\overline{x}_t$ with elements bounded by $\langle -1, 1\rangle$. Substituting (9) and $\overline{x}_t$ into (1), we can determine transformed variables $\overline{A}_t$, $\overline{Q}$, and $\overline{R}$.

Establishing bounds on the variance $\overline{P}_t$ of the transformed estimate $\hat{\overline{x}}_t$ is harder. Note that, substituting (3) into (2) for $\omega_{me} = 0$, the predictive variance of ϑ_e is

$$S_{\vartheta,t+1} = P_{\vartheta,t} + 2\Delta t P_{\vartheta\omega,t} + \Delta t^2 P_{\omega,t} + Q_\vartheta. \tag{10}$$

When the predicted output is close to the observations $\hat{y}_t \approx y_t$, $P_{\vartheta,t+1} \approx S_{\vartheta,t+1}$ in the correction step (4) and thus growing linearly with time without any bounds. This corresponds to the fact that the posterior density on ϑ_e is approaching uniform density, which is approximated by a Gaussian truncated at interval $\langle -1, 1\rangle$. The uniform density is obtained when $P_{\vartheta,t} \to \infty$. This is unacceptable for numerical representation, and an upper bound on $P_{\vartheta,t}$ must be set. Approximation of the uniform density for various choices on the upper bound is shown in Fig. 1.

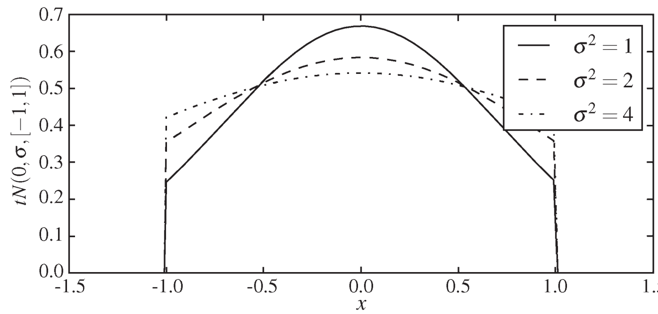

Fig. 1. Illustration of truncated normal density with zero mean and different variance σ^2.

The choice of the upper bound on diagonal elements of P_t is then a tradeoff between the accuracy of approximation of $P_{\vartheta,t}$ and the accuracy of approximation of the other elements. After this choice, the covariance matrix can be also transformed into

$$\overline{P}_{\vartheta,t} = \frac{P_{\vartheta,t}}{P_{\vartheta,\max}} \in \langle 0, 1\rangle. \tag{11}$$

The scaling allows one to choose robust initial conditions

$$\hat{x}_0 = [0,0,0,0] \qquad P_0 = \mathrm{diag}\left([1,1,1,1]\right). \tag{12}$$

Due to the restrictions of symmetry and positive definiteness, all remaining elements of matrix P_t are guaranteed to be within $\langle -P_{\vartheta,\max}, P_{\vartheta,\max}\rangle$. This is also true for the Cholesky decomposition, where all elements are within $\langle -\sqrt{P_{\vartheta,\max}}, \sqrt{P_{\vartheta,\max}}\rangle$. However, the situation is more complicated for the UD transformation, where the elements of U_t are ratios of the elements of matrix P_t. Hence, the range of all possible values is much higher. In our implementation, we avoid this problem by choosing the bounds for all elements of U_t, $U_{i,j,t} \in \langle -U_{t,\max}, U_{t,\max}\rangle$, and truncating all values that are outside this interval. This, however, adds additional computational complexity to the algorithm and further degrades the accuracy of estimation.

B. Algorithmic Changes

The algorithms presented in [30] are optimized for floating-point implementations. Some of these optimizations cannot be used in the fixed-point implementation since temporary variables would have poorly defined ranges. This problem is illustrated in the algorithms in Fig. 2. Note that the temporary variable `gamma` in the floating-point implementation is avoided since its dynamic range is high and its representation in a fixed-point would be inaccurate. Therefore, division by `alpha` that is done only once in the floating-point implementation (line 6) is performed `j` times in the fixed-point (line 12). Other routinely

```
gamma = 1/alpha;
for (j=0;j<dim;j++){
    beta   = alpha;
    alpha  +=  a[j]*b[j];
    lambda = -a[j]*gamma;
    gamma  = 1.0/alpha;
    D(j) *= beta*gamma;


    for (i=0;i<j;i++){
        beta   = U[i,j];
        U[i,j] += b[i]*lambda;
        b[i]   += b[j]*beta;
    }
}
```

```

for (j=0; j<dimx; j++) {
    zeta=alpha;
    alpha  += ((int32)a[j]*b[j])>>15;



    D[j] = ((int32)zeta*D[j])/alpha;
    if (D[j]==0) D[j]=1;

    for (i=0; i<j; i++) {
        beta  =  U[i,j];
        U[i,j]-= ((int32)a[j]*b[i])/zeta;
        b[i]  += ((int32)beta*b[j])>>15;
    }
}
```

Fig. 2. Comparison of (left) floating-point and (right) fixed-point implementations of a part of the Bierman–Thorton algorithm. Optimized access to indexed array elements that are used in the actual implementation is avoided for clarity.

used ways of computing algebraic expressions in fixed-point arithmetic also increase the numbers of multiplications and additions over the number of operations in the floating-point implementation.

C. Tuning of Covariance Matrices

It is well known that tuning of the covariance matrices of the EKF is a serious problem. Up to now, there does not exist any generally accepted automatic tuning procedure for sensorless controlled ac motor drives. This problem is even more demanding in fixed-point arithmetics, where even well-known facts—such as the dependence of the Kalman gain only on the ratio of matrices Q and R—have to be questioned. Specifically, choosing greater values of $\overline{R}$ implies greater values of $\overline{Q}$, which will cause faster saturation in (10). This can be compensated either by an increase of the upper bound on $S_{\vartheta,t}$ or by choosing very small values of both $\overline{Q}$ and $\overline{R}$. Since it is hard to analyze the consequences exactly, we have tuned the values of $\overline{R}$ and $\overline{Q}$, as well as their fixed-point ranges, experimentally.

D. Special Features of PMSM Drive

The considered model of the PMSM drive has the following special features.

1) Matrix A_t is rather sparse. This property could be used in computation of products A_tU_t and A_tG_t; however, the savings are so small that we do not implement it. The sparsity is advantageous for the Givens algorithm since it reduces the number of necessary rotations.
2) Matrix C is the identity matrix complemented by zeros. This property is equally advantageous for all algorithms, since multiplication CP_tC^{T} is replaced by a selection of the relevant part of matrix P_t.
3) Matrices Q and R are diagonal. This simplifies the computation of all algorithms since addition of zeros can be skipped.
4) Matrix P_t should be artificially truncated. The advantage in this case is with the algorithms based on the Cholesky decomposition, since its upper bound is a square root of the maximum, allowing one to represent higher dynamic range.

TABLE I
COMPARISON OF COMPUTATIONAL COMPLEXITY OF ALL CONSIDERED VARIANTS OF THE EKF FILTER IN FIXED-POINT IMPLEMENTATION

		*	+	/	$\sqrt{}$
full	prediction	$2n^3$	$2n^3+n$		
	correction	$2n^2+8n+2$	$2n^2+6n+3$	4	
UD	AU	n^2-3n+2	n^2-3n+2		
	Thorton	$\frac{4n^3+n^2-n}{2}$	$\frac{4n^3+n^2+2.5n}{3}$	$\frac{n^2-n}{2}$	
	Bierman	$2n^2+10n+2$	$2n^2+6n$	$4n$	
Cholesky	AG	n^2-n	n^2-n		
	Givens	$rO(n)$	$rO(n)$	$2r$	r
	Householder	n^3+5n^2+4n	n^3+5n^2+5n	$\frac{n^3+3n^2+2n}{2}$	n
	Carlson	$2n^2+5n$	$\frac{3n^2+9n}{2}$	$\frac{n^2+3n}{2}$	n

n denotes dimensionality of x_t, r is the number of required rotations, and $O(n)$ denotes number of operation linearly growing with n

All of these simplifications were taken into account, and the number of operations required for each algorithm is now summarized in Table I.

Exact comparison of these algorithms would require one to know the relative cost of all operations and to determine the number of rotations in the Givens algorithm. In our implementation, this is checked online in DSP, and it may slightly differ for each computational cycle. The maximum number of rotations for system (1) was 15, which implies relatively low numbers of multiplications and additions but higher number of $\mathrm{sqrt}()$ operations than that of the Householder variant. The price of the $\mathrm{sqrt}()$ operation is often the reason why variants based on the Cholesky decompositions are avoided.

However, the number of numerical operations is only a part of the algorithm where copy operations, comparisons, and function calls are also performed. Therefore, the total time of execution for each algorithm will be measured in Section IV.

IV. TESTS OF PROPOSED SQUARE-ROOT EKF ON PMSM DRIVE PROTOTYPE

The configuration of the investigated sensorless drive control is shown in Fig. 3. The drive control is based on the conventional vector control in Cartesian coordinates in the rotating reference frame (d, q) linked to a rotor flux linkage vector.

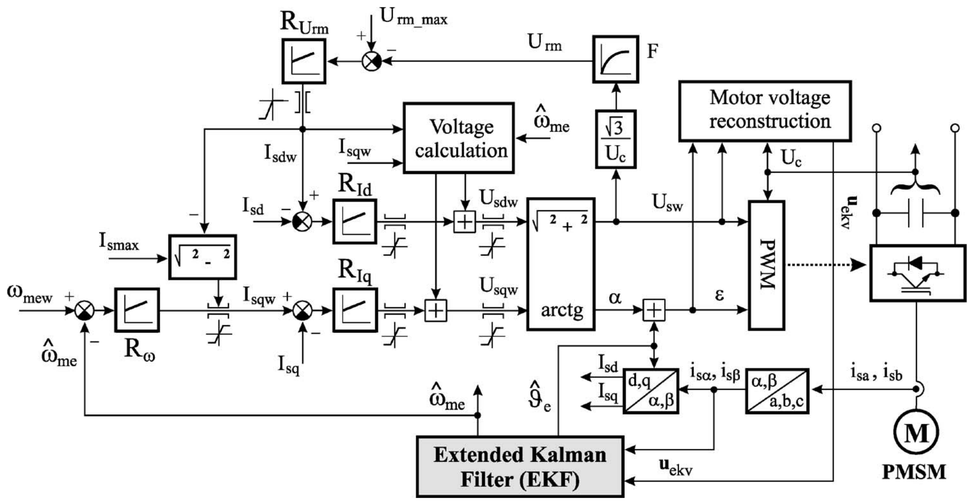

Fig. 3. Investigated sensorless control of a PMSM drive with the EKF.

TABLE II
MEASURED EXECUTION TIME OF VARIANTS OF THE EKF ON DSP (TEXAS INSTRUMENTS, TMS320F2812) WITH A CLOCK FREQUENCY OF 150 MHz

	time in μs
Full matrices	78
Bierman-Thorton	77
Carlson-Schmidt-Givens	80
Carlson-Schmidt-Householder	131

An input to the drive controller is the commanded electrical rotor speed ω_{mew} which is controlled by a proportional–integral (PI) controller R_ω. The output of R_ω is the demanded torque component I_{sqw} of the stator current vector. The torque (I_{sqw}) and flux (I_{sdw}) currents are controlled by PI controllers $R_{\rm Isq}$ and $R_{\rm Isd}$, respectively. Flux weakening is secured by PI controller $R_{\rm Urm}$ which controls the modulation depth (signal U_{rm}) of pulsewidth modulation (PWM) and commands the flux current I_{sdw}. The current controllers are supported by block "voltage calculation" (often referred to as "decoupling") which computes the components of the required stator voltage vector in the (d, q) frame using a simplified model of the PMSM in steady state. The components of the stator current vector $(i_{s\alpha}, i_{s\beta})$ and the reconstructed stator voltage vector u_{ekv} in the stationary reference frame are the inputs to the EKF. The stator voltage vector is reconstructed from the measured dc-link voltage and the known switching combination of the voltage-source converter. The EKF output is the estimated electrical rotor speed $\hat{\omega}_{me}$ and the electrical rotor position $\hat{\vartheta}_e$. The voltage-source converter employs a third-harmonic injected PWM with a carrier frequency of 4 kHz. The sampling period of the EKF, as well as that of the drive control, has been set to 125 μs.

The proposed sensorless drive control with all studied algorithms of the square-root EKF has been tested on a laboratory PMSM drive of rated power of 10.7 kW with parameters of the PMSM equivalent circuit: $R_s = 0.28\ \Omega$, $L_s = 3.465$ mH, $\Psi_{\rm pm} = 0.1989$ Wb, and four pole pairs. The proposed control and the EKF algorithms presented in Fig. 2 have been implemented in a fixed-point DSP (Texas Instruments, TMS320F2812). Execution times of all variants of the EKF measured with a DSP clock frequency of 150 MHz are displayed in Table II. Since the sampling period of the vector control, as well as that of the EKF, has been selected as 125 μs, the Householder algorithm was excluded from all other tests, because it was unable to provide the estimates within the required time.

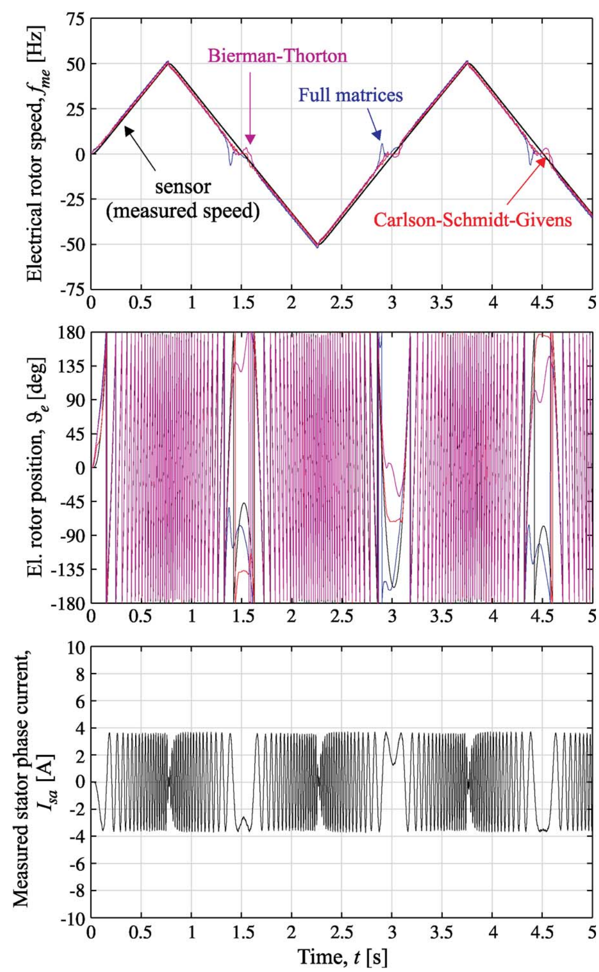

Fig. 4. Comparison of investigated EKF algorithms: Speed reversal, triangular speed profile, and commanded electrical rotor speed of $f_{mew} = \pm 50$ Hz.

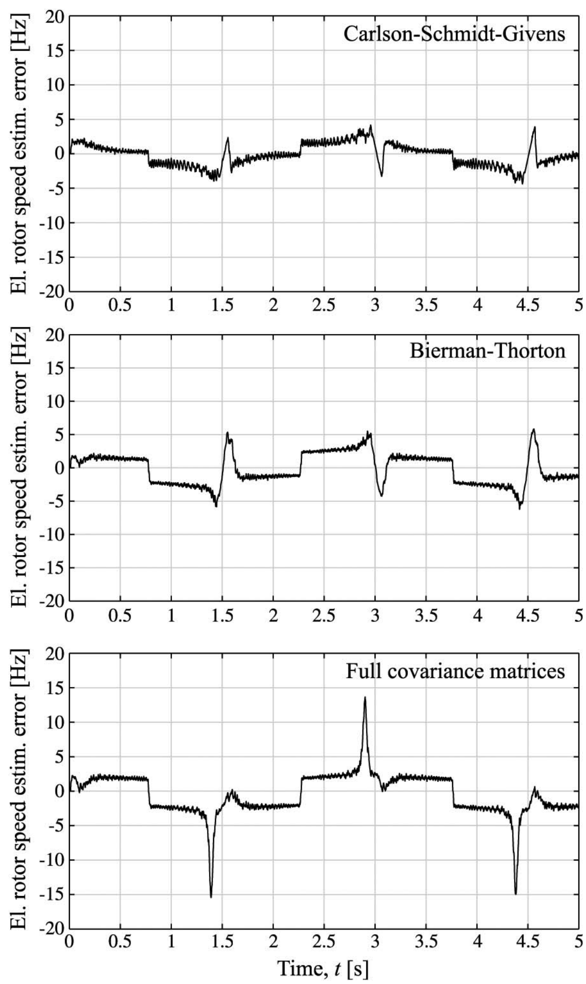

Fig. 5. Error of electrical rotor speed estimation for all investigated EKF algorithms: simulation scenario shown in Fig. 4.

A. Simulation Results

A simulation model of the PMSM drive has been designed and implemented in the C language. The "physical" model of a surface-mounted PMSM is represented by a state-space model in the stationary reference frame which has been solved using Adams–Bashforth difference formula of fourth order with a sampling period of 1 μs. The voltage-source inverter model respects as close as possible dead-time effects (the dead times have been set to 3 μs, which corresponds to those of the laboratory prototype) and nonlinear voltage drops on the power electronics devices (the power devices are modeled using approximations of their $V-A$ characteristics). The implemented control strategy and the EKF algorithms respect the behavior of a real microcontroller-based control system including realistic sampling, known transport delays, and finite calculation times. The sampling period of the control and EKF has been, as defined earlier, set to 125 μs.

Fig. 4 shows the behavior of all investigated EKF algorithms under the speed reversal effect. The drive was operated in the sensored mode, i.e., the control employed rotor speed and position feedback from the rotor position sensor. All EKF algorithms were computed during the simulation test in parallel. Errors of estimation of the electrical rotor speed by particular EKF algorithms are shown in Fig. 5. From the presented simulation results, it can be concluded that the Carlson–Schmidt–Givens algorithm achieved the best result. The speed estimation error is below five electrical degrees in the entire speed range, including critical low speeds. The conventional EKF with full covariance matrices had the biggest speed estimation error; the simulation presents peaks typical for this algorithm in estimation around zero speed.

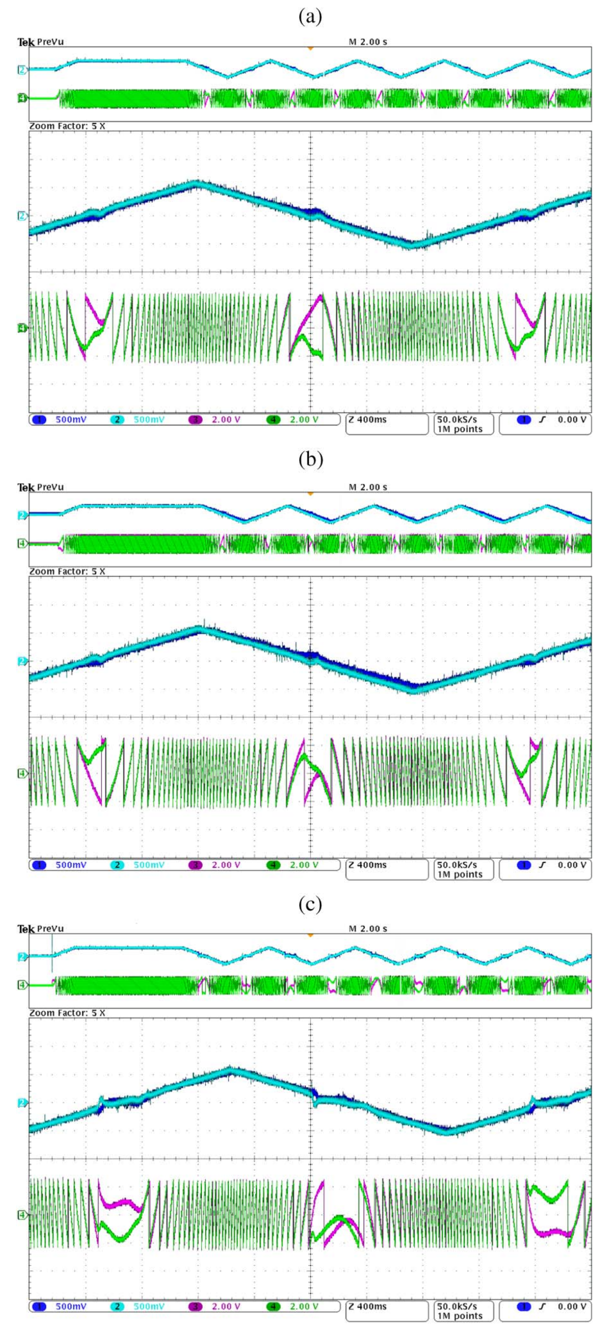

Fig. 6. Speed reversal: Triangular speed profile and commanded electrical rotor speed $f_{mew} = \pm 50$ Hz. ch1: Electrical rotor speed (sensor) [40 Hz/div]. ch2: Estimated electrical rotor speed (EKF) [40 Hz/div]. ch3: Electrical rotor position (sensor) [144°/div]. ch4: Estimated electrical rotor position (EKF) [144°/div]. Time scale: 400 ms/div. (a) Carlson–Schmidt–Givens implementation of EKF. (b) Bierman–Thorton implementation of EKF. (c) Full matrix implementation of EKF.

(a)

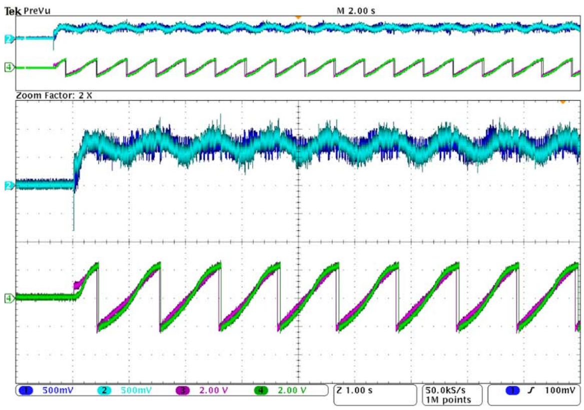

(b)

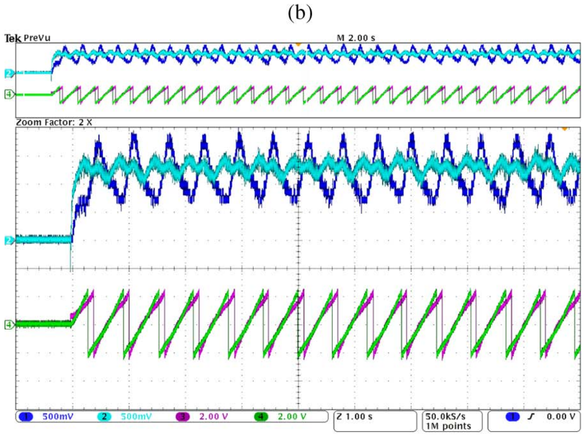

(c)

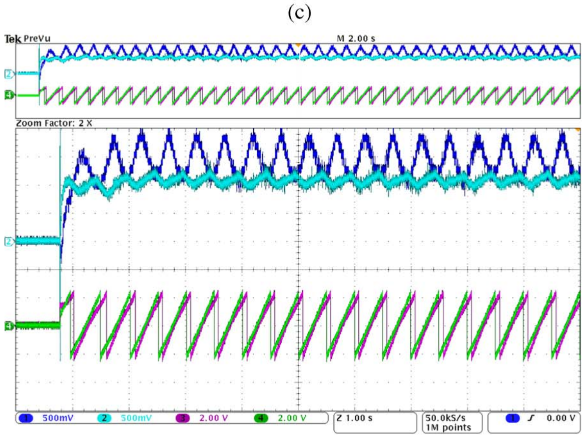

Fig. 7. Step change of electrical rotor speed f_{mew}: Initial rotor position is different from the EKF initial condition (12). ch1: Electrical rotor speed (sensor) [0.625 Hz/div]. ch2: Estimated electrical rotor speed (EKF) [0.625 Hz/div]. ch3: Electrical rotor position (sensor) [144°/div]. ch4: Estimated electrical rotor position (EKF) [144°/div]. Time scale: 1 s/div. (a) Carlson–Schmidt–Givens implementation of EKF; commanded electrical rotor speed of $f_{mew} = 0 \rightarrow 1$ Hz. (b) Bierman–Thorton implementation of EKF; commanded electrical rotor speed of $f_{mew} = 0 \rightarrow 1.8$ Hz. (c) Full matrix implementation of EKF; commanded electrical rotor speed of $f_{mew} = 0 \rightarrow 1.5$ Hz.

B. Experimental Results

The behavior of the investigated drive control under the speed reversal effect for all three variants of the EKF is documented in Fig. 6. The drive was operated in the sensorless mode under a triangular speed profile with the commanded electrical rotor speed of $f_{mew} = \pm 50$ Hz. We have employed quite slow speed ramp to verify the properties of the analyzed EKF algorithms in the critical low-speed region. It can be concluded that the Carlson–Schmidt–Givens and the Bierman–Thorton algorithm achieved better results than the conventional EKF with full covariance matrices. Both square-root algorithms achieved very good steady-state precision and cultivated transitions through the low-speed region with only a small peak on the estimated electrical rotor speed around zero. In the next test (Fig. 7), we have tested the capabilities of the investigated EKF algorithms in the low-speed region. The drive was operated again in the sensorless mode, and the PMSM was not mechanically loaded. The Carlson–Schmidt–Givens algorithm was able to secure stable drive operation at an electrical rotor speed of 1 Hz (i.e., a mechanical rotor speed of 15 r/min). The conventional EKF algorithm with full covariance matrices was able to secure stable drive operation around an electrical rotor speed of 1.5 Hz but introduced a steady-state error in the rotor speed estimation. The worst result was achieved by the Bierman–Thorton algorithm, which started its stable operation around 1.8 Hz. However, the steady-state error in the rotor speed estimation was, in contrast to the conventional EKF, equal to zero.

V. Conclusion

Three variants of square-root implementations of the EKF equations were compared with the standard implementation with full matrix representation in sensorless control of an ac motor drive. We found that the Carlson–Schmidt–Householder has to be excluded from tests on a laboratory prototype because it was too computationally expensive to run in the chosen sampling period. Hence, only Bierman–Thorton and Carlson–Schmidt–Givens variants were tested for numerical accuracy and robustness in critical operating regimes of the drive. Under speed reversal, both square-root algorithms significantly improve the accuracy of estimation over the standard implementation. In low-speed operation, the Carlson–Schmidt–Givens algorithm was capable of reliable operation from an electrical rotor speed of 1 Hz, while the standard implementation and Bierman–Thorton algorithms operated above 1.5 and 1.8 Hz, respectively. For the particular PMSM drive, the Carlson–Schmidt–Givens algorithm offers the best overall performance. The computational cost of the square-root EKF is slightly higher than that of the conventional algorithm. This conclusion is in agreement with the findings for square-root methods in other applications. However, the main benefits of the square-root EKF are improved accuracy and robustness in critical operating conditions of the drive. Since other types of ac motor drives have similar model structure, the methods can improve the quality of fixed-point implementations of all EKF-based sensorless drive control.

References

[1] Q. Gao, G. Asher, M. Sumner, and L. Empringham, “Position estimation of a matrix-converter-fed AC PM machine from zero to high speed using PWM excitation,” *IEEE Trans. Ind. Electron.*, vol. 56, no. 6, pp. 2030–2038, Jun. 2009.

[2] R. Raute, C. Caruana, C. S. Staines, J. Cilia, M. Sumner, and G. M. Asher, “Analysis and compensation of inverter nonlinearity effect on a sensorless PMSM drive at very low and zero speed operation,” *IEEE Trans. Ind. Electron.*, vol. 57, no. 12, pp. 4065–4074, Dec. 2010.

[3] J. Holtz, "Sensorless position control of induction motors—An emerging technology," *IEEE Trans. Ind. Electron.*, vol. 45, no. 6, pp. 840–851, Dec. 1998.
[4] J. Holtz and H. Pan, "Acquisition of rotor anisotropy signals in sensorless position control systems," *IEEE Trans. Ind. Appl.*, vol. 40, no. 5, pp. 1379–1387, Sep./Oct. 2004.
[5] H. De Kock, M. Kamper, and R. Kennel, "Anisotropy comparison of reluctance and PM synchronous machines for position sensorless control using HF carrier injection," *IEEE Trans. Power Electron.*, vol. 24, no. 8, pp. 1905–1913, Aug. 2009.
[6] M. Pucci and C. Serporta, "Finite-element analysis of rotor slotting saliency in induction motors for sensorless control," *IEEE Trans. Magn.*, vol. 46, no. 2, pp. 650–653, Feb. 2010.
[7] R. Leidhold, "Position sensorless control of PM synchronous motors based on zero-sequence carrier injection," *IEEE Trans. Ind. Electron.*, vol. 58, no. 12, pp. 5371–5379, Dec. 2011.
[8] M. Preindl and E. Schaltz, "Sensorless model predictive direct current control using novel second-order PLL observer for PMSM drive systems," *IEEE Trans. Ind. Electron.*, vol. 58, no. 9, pp. 4087–4095, Sep. 2011.
[9] J. Holtz and J. Quan, "Sensorless vector control of induction motors at very low speed using a nonlinear inverter model and parameter identification," *IEEE Trans. Ind. Appl.*, vol. 38, no. 4, pp. 1087–1095, Jul./Aug. 2002.
[10] C. Lascu, I. Boldea, and F. Blaabjerg, "A class of speed-sensorless sliding-mode observers for high-performance induction motor drives," *IEEE Trans. Ind. Electron.*, vol. 56, no. 9, pp. 3394–3403, Sep. 2009.
[11] J. Jiang and J. Holtz, "High dynamic speed sensorless ac drive with online model parameter tuning for steady-state accuracy," *IEEE Trans. Ind. Electron.*, vol. 44, no. 2, pp. 240–246, Apr. 1997.
[12] I. Boldea, M. Paicu, G.-D. Andreescu, and F. Blaabjerg, "'Active flux' DTFC-SVM sensorless control of IPMSM," *IEEE Trans. Energy Convers.*, vol. 24, no. 2, pp. 314–322, Jun. 2009.
[13] T. Orlowska-Kowalska and M. Dybkowski, "Robust speed-sensorless induction motor drive for traction applications," in *Proc. 36th Annu. Conf. IEEE Ind. Electron. Soc.*, 2010, pp. 2358–2363.
[14] T. Orlowska-Kowalska and M. Dybkowski, "Stator-current-based MRAS estimator for a wide range speed-sensorless induction-motor drive," *IEEE Trans. Ind. Electron.*, vol. 57, no. 4, pp. 1296–1308, Apr. 2010.
[15] K. Jezernik and M. Rodic, "High precision motion control of servo drives," *IEEE Trans. Ind. Electron.*, vol. 56, no. 10, pp. 3810–3816, Oct. 2009.
[16] P. Brandstetter, O. Francik, and P. Simonik, "AC drive with permanent magnet synchronous motor and sensorless control," in *Proc. EPE/PEMC*, 2010, pp. T2-66–T2-71.
[17] S. Bolognani, R. Oboe, and M. Zigliotto, "Sensorless full-digital PMSM drive with EKF estimation of speed and rotor position," *IEEE Trans. Ind. Electron.*, vol. 46, no. 1, pp. 184–191, Feb. 1999.
[18] S. Bolognani, M. Zigliotto, and M. Zordan, "Extended-range PMSM sensorless speed drive based on stochastic filtering," *IEEE Trans. Power Electron.*, vol. 16, no. 1, pp. 110–117, Jan. 2001.
[19] M. Barut, S. Bogosyan, and M. Gokasan, "Experimental evaluation of braided EKF for sensorless control of induction motors," *IEEE Trans. Ind. Electron.*, vol. 55, no. 2, pp. 620–632, Feb. 2008.
[20] M. Boussak, "Implementation and experimental investigation of sensorless speed control with initial rotor position estimation for interior permanent magnet synchronous motor drive," *IEEE Trans. Power Electron.*, vol. 20, no. 6, pp. 1413–1422, Nov. 2005.
[21] Y.-H. Kim and Y.-S. Kook, "High performance IPMSM drives without rotational position sensors using reduced-order EKF," *IEEE Trans. Energy Convers.*, vol. 14, no. 4, pp. 868–873, Dec. 1999.
[22] M. Hilairet, F. Auger, and E. Berthelot, "Speed and rotor flux estimation of induction machines using a two-stage extended Kalman filter," *Automatica*, vol. 45, no. 8, pp. 1819–1827, Aug. 2009.
[23] K. Szabat, T. Orlowska-Kowalska, and M. Dybkowski, "Indirect adaptive control of induction motor drive system with an elastic coupling," *IEEE Trans. Ind. Electron.*, vol. 56, no. 10, pp. 4038–4042, Oct. 2009.
[24] L. Idkhajine and E. Monmasson, "Design methodology for complex FPGA-based controllers—Application to an EKF sensorless AC drive," in *Proc. ICEM*, 2010, pp. 1–6.
[25] Z. Peroutka, "Development of sensorless PMSM drives: Application of extended Kalman filter," in *Proc. IEEE Int. Symp. Ind. Electron.*, Dubrovnik, Croatia, 2005, pp. 1647–1652.
[26] Z. Peroutka, "Design considerations for sensorless control of PMSM drive based on extended Kalman filter," in *Proc. 11th EPE*, Dresden, Germany, 2005, pp. 1–10.
[27] N. Salvatore, A. Caponio, F. Neri, S. Stasi, and G. Cascella, "Optimization of delayed-state Kalman-filter-based algorithm via differential evolution for sensorless control of induction motors," *IEEE Trans. Ind. Electron.*, vol. 57, no. 1, pp. 385–394, Jan. 2010.
[28] A. Akrad, M. Hilairet, and D. Diallo, "Design of a fault-tolerant controller based on observers for a PMSM drive," *IEEE Trans. Ind. Electron.*, vol. 58, no. 4, pp. 1416–1427, Apr. 2011.
[29] R. Dhaouadi, N. Mohan, and L. Norum, "Design and implementation of an extended Kalman filter for the state estimation of a permanent magnet synchronous motor," *IEEE Trans. Power Electron.*, vol. 6, no. 3, pp. 491–497, Jul. 1991.
[30] M. Grewal and A. Andrews, *Kalman Filtering: Theory and Practice Using MATLAB*. Hoboken, NJ: Wiley-IEEE Press, 2008.
[31] M. Grewal and J. Kain, "Kalman filter implementation with improved numerical properties," *IEEE Trans. Autom. Control*, vol. 55, no. 9, pp. 2058–2068, Sep. 2010.
[32] Z. Peroutka, K. Zeman, F. Krus, and F. Kosta, "New generation of trams with gearless wheel PMSM drives: From simple diagnostics to sensorless control," in *Proc. EPE/PEMC*, 2010, pp. S10-31–S10-36.
[33] Z. Peroutka, V. Šmídl, and D. Vošmik, "Challenges and limits of extended Kalman filter based sensorless control of permanent magnet synchronous machine drives," in *Proc. 13th Eur. Conf. Power Electron. Appl.*, Barcelona, Spain, 2009, pp. 1–11.
[34] T. Bak, R. Wisniewski, and M. Blanke, "Autonomous attitude determination and control system for the Ørsted satellite," in *Proc. IEEE Aerosp. Appl. Conf.*, 1996, vol. 2, pp. 173–186.

Václav Šmídl (M'05) received the M.S. degree in control engineering from the University of West Bohemia, Plzeň, Czech Republic, in 1999 and the Ph.D. degree in electrical engineering from Trinity College Dublin, Dublin, Ireland, in 2004.

Since 2004, he has been a Researcher with the Institute of Information Theory and Automation, The Academy of Sciences of the Czech Republic, Prague, Czech Republic. Since October 2010, he has been with the Regional Innovation Centre for Electrical Engineering, University of West Bohemia. He published one research monograph, five journal papers, and over 40 conference papers. His research interests are advanced estimation and control techniques and their applications.

Zdeněk Peroutka (S'01–M'04) received the M.S. and Ph.D. degrees in electrical engineering from the University of West Bohemia (UWB), Plzeň, Czech Republic, in 2000 and 2004, respectively.

From 2004 to 2006, he was an Assistant Professor with UWB, where he has been an Associate Professor and the Head of the Section of Power Electronics and Control Systems since 2006, the Vice-Dean for Science and Strategy and the Deputy Dean of the Faculty of Electrical Engineering since March 2010, and the Scientific Director and a Principal Investigator of the Regional Innovation Centre for Electrical Engineering since October 2010. He published more than 80 papers in international journals and conferences. He is an inventor of two patents and two utility models. His research activities concern power electronics, electrical drives, and control theory. His main research topic is control of drives of modern transport systems and vehicles, and power electronics converters for medium-voltage applications. His recent research activities are focused on sensorless control of ac motor drives.

Dr. Peroutka is a member of the European Power Electronics and Drives (EPE) Association. He was a recipient of several national and international awards, for example, Best Paper awards in EPE-Power Electronics and Motion Control (PEMC) 2006, Electrical Drives and Power Electronics 2007, and EPE-PEMC 2010 conferences.